

College of Earth and Mineral Sciences

PENNSTATE



DEPARTMENT OF MATERIALS SCIENCE

METALLURGY PROGRAM

AD-A188 071

TECHNICAL REPORT

October 1, 1987

OFFICE OF NAVAL RESEARCH

Contract No. N00014-84-k-0201

IR DROPS AND THE LOCAL ELECTRODE POTENTIAL
DURING CREVICING OF IRON

Howard W. Pickering

Department of Materials Science & Engineering
The Pennsylvania State University

DTIC
ELECTE
NOV 16 1987
S D

DISTRIBUTION STATEMENT A

Approved for public release;
Distribution Unlimited

PENN STATE

College of Earth and Mineral Sciences

Undergraduate Majors

Ceramic Science and Engineering, Fuel Science, Metals Science and Engineering, Polymer Science; Mineral Economics; Mining Engineering, Petroleum and Natural Gas Engineering; Earth Sciences, Geosciences; Geography; Meteorology.

Graduate Programs and Fields of Research

Ceramic Science and Engineering, Fuel Science, Metals Science and Engineering, Polymer Science; Mineral Economics; Mining Engineering, Mineral Processing, Petroleum and Natural Gas Engineering; Geochemistry and Mineralogy, Geology, Geophysics; Geography; Meteorology.

Universitywide Interdisciplinary Graduate Programs Involving EMS Faculty and Students

Earth Sciences, Ecology, Environmental Pollution Control Engineering, Mineral Engineering Management, Solid State Science.

Associate Degree Programs

Metallurgical Engineering Technology (Shenango Valley Campus).

Interdisciplinary Research Groups Centered in the College

C. Drew Stahl Center for Advanced Oil Recovery, Center for Advanced Materials, Coal Research Section, Earth System Science Center, Mining and Mineral Resources Research Institute, Ore Deposits Research Group.

Analytical and Characterization Laboratories (Mineral Constitution Laboratories)

Services available include: classical chemical analysis of metals and silicate and carbonate rocks; X-ray diffraction and fluorescence; electron microscopy and diffraction; electron microprobe analysis; atomic absorption analysis; spectrochemical analysis; surface analysis by secondary ion mass spectrometry (SIMS); and scanning electron microscopy (SEM).

The Pennsylvania State University, in compliance with federal and state laws, is committed to the policy that all persons shall have equal access to programs, admission, and employment without regard to race, religion, sex, national origin, handicap, age, or status as a disabled or Vietnam-era veteran. Direct all affirmative action inquiries to the Affirmative Action Officer, Suzanne Brooks, 201 Willard Building, University Park, PA 16802; (814) 863-0471.
U Ed. 87-1027
Produced by the Penn State Department of Publications

REPORT DOCUMENTATION PAGE		READ INSTRUCTIONS BEFORE COMPLETING FORM
1. REPORT NUMBER Technical Report, Oct. 2, 1987	2. GOVT ACCESSION NO.	3. RECIPIENT'S CAT. LOG NUMBER A188071
4. TITLE (and Subtitle) IR DROPS AND THE LOCAL ELECTRODE POTENTIAL DURING CREVICING OF IRON		5. TYPE OF REPORT & PERIOD COVERED Technical Report
		6. PERFORMING ORG. REPORT NUMBER
7. AUTHOR(s) H. W. Pickering		8. CONTRACT OR GRANT NUMBER(s) N00014-84-k-0201
9. PERFORMING ORGANIZATION NAME AND ADDRESS Metallurgy Program, 209 Steidle Building The Pennsylvania State University University Park, PA 16802		10. PROGRAM ELEMENT, PROJECT, TASK AREA & WORK UNIT NUMBERS
11. CONTROLLING OFFICE NAME AND ADDRESS		12. REPORT DATE October 1, 1987
		13. NUMBER OF PAGES
14. MONITORING AGENCY NAME & ADDRESS (if different from Controlling Office)		15. SECURITY CLASS. (of this report)
		15a. DECLASSIFICATION/DOWNGRADING SCHEDULE
16. DISTRIBUTION STATEMENT (of this Report)		
17. DISTRIBUTION STATEMENT (of the abstract entered in Block 20, if different from Report)		
18. SUPPLEMENTARY NOTES		
19. KEY WORDS (Continue on reverse side if necessary and identify by block number)		
20. ABSTRACT (Continue on reverse side if necessary and identify by block number) In this work a traditionally misregarded point of view, a different electrode potential within the cavity than exists at the outer surface, is shown to be of great importance for the occurrence of localized corrosion in crevices. Based on the results of this work crevice corrosion is concluded to occur due to an electrode potential in the crevice that is in the active loop region of the polarization curve of the crevice electrolyte. Compositional effects were not significantly involved since the solution did not contain Cl^- or other aggressive ions and a buffer solution was used to minimize pH changes. Gas		

DD FORM 1 JAN 73 1473

EDITION OF 1 NOV 65 IS OBSOLETE
S/N 0102-014-6601

20. ABSTRACT con't.

bubble accumulation in the crevice increases the rate of crevicing and can initiate a new crevicing action at the metal-gas-electrolyte interface even on otherwise passivated surfaces. These results were obtained for an iron sample containing a preexisting crevice in a buffer 0.5 M sodium acetate - 0.5 M acetic acid solution of pH 4.6. In some experiments an inhibitor, sodium chromate, was present in the solution in order to observe the potential variation for an inactive crevice.

IR DROPS AND THE LOCAL ELECTRODE POTENTIAL DURING CREVICING OF IRON

Alberto Valdes and Howard W. Pickering
The Pennsylvania State University
Department of Materials Science and Engineering
University Park, PA 16802, USA

ABSTRACT

In this work a traditionally disregarded point of view, a different electrode potential within the cavity than exists at the outer surface, is shown to be of great importance for the occurrence of localized corrosion in crevices. Based on the results of this work crevice corrosion is concluded to occur due to an electrode potential in the crevice that is in the active loop region of the polarization curve of the crevice electrolyte. Compositional effects were not significantly involved since the solution did not contain Cl^- or other aggressive ions and a buffer solution was used to minimize pH changes. Gas bubble accumulation in the crevice increases the rate of crevicing and can initiate a new crevicing action at the metal-gas-electrolyte interface even on otherwise passivated surfaces. These results were obtained for an iron sample containing a preexisting crevice in a buffer 0.5 M sodium acetate - 0.5 M acetic acid solution of pH 4.6. In some experiments an inhibitor, sodium chromate, was present in the solution in order to observe the potential variation for an inactive crevice.

Approved For	
DATE	10/1/80
BY	10/1/80
per ltr.	
DATE	10/1/80
BY	10/1/80
A-1	

INSPECTED
&

INTRODUCTION

The magnitude of the potential drop that can be obtained in restricted environments such as pits, crevices and cracks has been an open controversy over the years. What this ongoing controversy indicates is that present day knowledge of the chemical and electrochemical conditions inside restricted environments is very limited and in need of more experimental study.

A common feature of all growing pits, crevices and cracks is a restricted mass and charge transport from the cavity to the bulk solution and viceversa. This results either in the accumulation of solid corrosion products or the entrapment of gas bubbles within the walls of the cavity, both of which can increase the IR drop. Solid corrosion products have received a fair amount of attention, see e.g. (1), but the effect of in-place gas bubbles, as well as solid corrosion products, on the electrode potential in a cavity has not been examined to its due extent, despite supporting experimental evidence, presented at the Williamsburg Conference and elsewhere, clearly showing a possible new approach to explaining pit and crevice initiation and growth (2,3). Papers reviewing these results have been published elsewhere (4,5) and also in this proceedings (6); therefore, no details will be presented here.

These data, that show cavity electrode potentials quite different from the potential at the outer passivated surface, are not consistent with traditional theories of localized corrosion. The latter invoke composition differences in the electrolyte as the cause of localized corrosion and in important ways ignore potential drops. Available mathematical models of localized corrosion and of stress corrosion cracking are also not complete since they do not predict the 10^3 mV potential drops that occur for some conditions. The exception is the model by Ateya and Pickering (9) that predicts a larger and larger potential drop as the crevice narrows; this model, developed for hydrogen evolution under cathodic polarization conditions, can be qualitatively applied to localized corrosion conditions.

The experiments described in this paper are designed to study the role of IR drops on crevice corrosion under conditions that minimize changes in composition of the crevice electrolyte. The extent and nature of crevicing in the absence of chloride ion and gas

accumulation are also investigated. Thus, the importance of large potential changes, rather than solution composition changes, in the occurrence of localized corrosion is stressed.

EXPERIMENTAL

The material used in this work was Ferrovac-E iron. The specimens were cut from bars, degreased, heat treated at 800°C for two hours and furnace cooled. The experiments were carried out at pH 4.6 in a solution of 0.5M acetic acid and 0.5M sodium acetate prepared with reagent grade chemicals and double distilled water. This is a buffer solution designed to minimize pH changes in the crevice. Sodium chromate was added to inhibit crevicing in some experiments.

The sample arrangement is shown in Figure 1. A specimen, after polishing to a mirror-like surface, was force fit into the TeflonTM holder and the Plexiglas plate was attached to one of its surfaces in order to form an artificial crevice between the Plexiglas and the metal wall. The crevice thus consisted of one metallic wall, four inert (Plexiglas) walls and one opening (5mm x 0.5 mm) to the bulk of the solution; its depth was 10 mm. The exposed outer (top) surface was 5 mm x 20 mm in area. Lacquer was used to eliminate crevices between the iron and Teflon.

The experimental set-up used to make the measurements included a Luggin capillary probe drawn to a diameter of less than 0.02 cm and is shown in Figure 2. The non-interference of the Luggin capillary probe on the observed behavior was satisfied in two ways: (a) the same experiments conducted in the absence of the probe yielded the same features of the crevicing process and (b) the occurrence of hydrogen evolution from within the crevice proved that the potential drop was in the range of those measured. In addition, Ateya and Pickering (9,10) obtained reproducible results when using a Luggin measuring probe with a diameter on the order of 0.01 cm to measure local potentials in an artificial crevice with the same dimensions as the one used in this work. Observation of the events inside the crevice and photographic recording of them were possible with a stereo microscope viewing the crevice through the Plexiglas plate (see Figure 1). Luggin capillaries connected to saturated calomel electrodes (SCE) were used to monitor the electrode potential at different positions inside the crevice and to control the (applied)

potential on the outside (top) surface. All of the experiments were carried out under potentiostatic control in solutions open to the atmosphere.

The experimental procedure was as follows: the sample was first placed in the empty cell and all the necessary arrangements were made. With the sample under cathodic protection (generally -1.0 V, SCE) the electrolyte was added; the cathodic polarization was maintained until a constant current was reached in order to assure the removal of any air-formed film prior to the application of the anodic polarization. Once these conditions were obtained, the test was started by switching the potential into the passive region. In some experiments the cathodic pretreatment was not used; in this case the potential was set in the passive region and then the electrolyte was added. All records were time related to the moment at which the anodic polarization was first applied. The measured current was presented as current density based on the total exposed metal area of 1.5 cm^2 (outer surface and crevice wall).

RESULTS AND DISCUSSION

Electrode Potentials in the Crevice

The electrode potential as a function of distance into the artificial crevice of an anodically polarized iron sample for gas-free and gas-occupied crevices are shown in Figure 3. A decrease in potential was found with an increase in the distance into the cavity in agreement with expected behaviour (2-5,10,11). At the opening of the crevice, the measured electrode potential is close to the applied potential; towards the bottom the electrode potential is at an almost constant value of -0.57/-0.58 (SCE). The corrosion rate was observed and measured to be high in a particular region of the negative potentials within the crevice; this is discussed below. For both gas-free and gas-occupied crevices, a large shift in potential occurs. When the shape of the bubble changed for any reason and did not fill completely the cross section, and even when the bubble was dislodged, the large magnitude of the potential change in the crevice was in general the same. The only difference was that the potential profile was more localized to the region of the bubble for a gas filled cross section (shadowed region in Figure 3). The quasi stationary current (1 hr value), however, was higher with the gas present, e.g., 4.5 mA cm^{-2} in the presence of the

gas vs. 2.0 mA cm^{-2} in the absence of the gas. Thus, even without in-place gas bubbles, large IR drops greater than the IR^* value in Figure 4, and currents that approach the maximum currents of the active loop, produce the crevicing. Since these densities were obtained from the measured current using the total 1.5 cm^2 of exposed iron (crevice wall and outer surface), the actual crevicing current density was roughly an order of a magnitude larger since the current was nearly completely from a narrow band just below the active/passive boundary on the crevice wall, as reported below.

Regarding the current flowing out of the crevice, the presence of a non-conductive medium (gas bubble) filling the cross section has the effect of a large resistance in the path of the current. The situation corresponds to the near isolation of the lower portion of the crevice from the bulk solution, the only available path for current flow and mass transport in and out of the crevice being the wedge shaped liquid regions between the bubble and the walls of the cavity (2-5). Similarly, wedge shaped liquid regions also exist between the bubble and the outside walls of the Luggin capillary probe when used to measure the local electrode potential underneath the bubble. These areas together add to a very small part of the entire cross section of the cavity and, as a result, only a very small cross sectional area is available for current flow. This reasoning is consistent with a modeling study of reactions in crevices that shows that the $IR > IR^*$ condition is more likely met the narrower is the crevice (9). Thus, even for a very small metal dissolution rate, a large IR can develop and cause the electrode potential in the wedge shaped region between the bubble and metal (microcrevice), and also below the bubble if the bubble occupies the entire cross section, to be below the passivation potential for the solution in the crevice (2,3). Gas bubble constrictions were found to be necessary for the $IR > IR^*$ condition (Figure 4) to be met during pitting of iron (2,3). In Valdes' experiments on crevicing of iron reported above, a shift of the electrode potential to near the limiting potential was obtained without the presence of gas constrictions because of the relatively long current path within the crevice as shown elsewhere (6).

Since, however, the potential profile in the crevice is similar with or without the gas accumulation (Figure 3), some other factor must cause the higher crevicing current in the presence of the gas. It is interesting to note that an increase in current is contrary to the usual response to an impedance (gas constriction). A more prominent active loop caused by changes in the solution composition in the region covered by the bubble could be involved. Alternatively, a larger area of the crevice wall could be a factor. In the absence of in-place gas, the high current region does not spread much below the active/passive transition. To do so would increase the average distance of current flow out of the crevice (either to the outer surface where the cathodic reaction mainly occurs under open circuit crevicing or to the auxiliary electrode in the case of crevicing during anodic protection). This is equivalent to the situation known to occur during galvanic corrosion of dissimilar metals in poorly conducting electrolytes, where a narrow deep penetration occurs in the more active metal just adjacent to the other metal on whose surface the cathodic reaction mainly occurs.

If an oxidant is also present within the crevice electrolyte, typically H^+ ions for crevicing of base metals, a more complex situation exists. In this case the oxidant can establish a mixed potential deep in the crevice where the influence of the primary oxidant mainly available at the outer surface (or the applied anodic protection) is relatively weak. The presence of an oxidant within the crevice also shifts the limiting potential, i_{LIM} , from the reversible potential of the metal dissolution reaction to the mixed potential established by the oxidant, as is discussed elsewhere (5,12). Also, reduction of the oxidant within the crevice tends to distribute the metal dissolution reaction over deeper portions of the crevice wall since current paths for this portion of the total metal dissolution current would be confined to relatively small distances within the crevice itself.

It will be shown in the rest of this paper that the active/passive interface and electrode potentials more negative than the active/passive value illustrated in Figure 4 are present in a crevice (1) that is supporting a local cell action but are not if the cell is inactive, and (2) for which $IR > IR^*$ even without gas or solid corrosion product accumulation. Additionally, it will be shown that a trapped gas bubble is capable of influencing and modifying the crevicing kinetics and

morphology of attack just below the active/passive interface, i.e. along the triple interface metal-gas-electrolyte.

Finding large potential drops in restricted environments is not new, as mentioned elsewhere in this proceedings (6). Other authors have reported them for various metals and environments, usually attributing their findings in some way to reduced mass transport due to an occluded corrosion cell. The nature of the occluded cell has also been clarified, being either solid or gaseous reaction products (2,3). Explanations of largely different stable electrode potentials along the crevice wall based on accumulated gas, advanced by previous workers (2,3,9) also can hold in the absence of the gas. $IR > IR^*$ can exist in crevices without accumulated gas because of the long current path, in contrast to the shorter paths in stable pitting of iron where gas or solid constrictions have been observed to be present when the measured potential within the pit was negative of the active/passive potential of the electrolyte in the pit (2-6). The idea, however, that only an active condition is needed within the crevice, advanced by various workers, is not adequate if part of the crevice wall next to the opening is passive. In this case it is clear that, in addition, an active/passive transition is required in the polarization curve of the crevice solution.

Calculated IR drops for the crevice used in this paper and the measured currents are easily as large as the measured IR values as shown elsewhere in this proceedings (6). This is true even for high conductivity electrolytes. In general, for high conductivity electrolytes, the conductivity of the crevice electrolyte is likely to be less than that of the bulk electrolyte, because of the gas voidage in the crevice solution. As is well known, a fraction of the total quantity of dissolved gas generated at an electrode is evolved in gaseous form directly at the electrode. Some of these gas bubbles will grow attached to the electrode causing a bubble curtain, whereas others will detach and move to the electrolyte phase. Of the latter, those that have the critical size for growth will grow to become large bubbles, whereas the ones smaller than the critical size will redissolve. It is then reasonable to expect a large population of microscopic bubbles in the liquid phase which can be thought of as a dispersion of the evolved gas in the electrolyte. Dispersions of gas in liquids show a decrease in the conductivity with an increase in the void fraction (13-19),

the reason being the increment in the proportion of the non-conducting material (gas) compared to the conducting material (electrolyte). Figure 5 illustrates the results of several theoretical models (20) where the ratio of the conductivity of dispersions of non-conductive spheres of unequal size to the conductivity of the continuous phase, is plotted versus the volume fraction of the dispersed phase. A good agreement has been found with experimental data (20).

The hydrogen evolution occurring in the crevice during the cathodic pre-treatment was very rapid. During such a process all sizes of bubbles grow and detach from the cavity, with a number of them easily visible because of their size, but a large number of bubbles in the very early stages of growth must also exist in solution. Although the volume of each bubble would be very small, summed together they would correspond to a large gas voidage in the cavity, thereby producing a lower solution conductivity. At the moment of switching the potential to the passive region hydrogen evolution ceases at the outer surface due to the new electrochemical condition and anodic currents commence. At the outer surface and in the outer part of the crevice wall, the anodic current will decrease as the surface passivates but deeper in the cavity the current remains high because $IR > IR^*$, i.e., the electrode potential is in the active region. In addition, hydrogen evolution was observed to continue within the crevice during anodic polarization indicating that some regions of the crevice wall are at potentials in the region of hydrogen evolution, in which case a low conductivity due to gas voidage is likely to exist.

Crevice Morphology and Rate

Figure 6 shows a photographic sequence of the events in a crevice after a potential in the passive region was applied to the outer (top) surface. In this experiment there was no significant gas accumulation in the crevice. In a short time a line representing an active/passive interface appeared (arrow), above which the crevice wall remained passive consistent with the measured potential in the passive region, and below which the active state was maintained consistent with measured potentials in the active region as described above and illustrated in Figure 4. The occurrence of stable active dissolution below this line is evidenced by the loss of the original metallic gloss which, on the other hand, is still observable above the interface. This active/passive

boundary initially moves upward as some of the already passivated surface becomes active. The rate of metal dissolution is high in a region identified by a bracket just below the active/passive transition in the ten minute photograph of Figure 6. Electrode potential measurements reported in Figure 3 show this (bracket) region of the crevice wall to correspond to the high current portion of the active loop of the polarization curve (Figure 4). With the highest dissolution rate occurring in this region, a new crevice appears with time, as illustrated in the upper sketch in Figure 4. After ten minutes (Figure 6) enough metal has been dissolved to make evident the start of a local penetration (referred to as the active crevicing site) in this region of the cavity wall. After a longer time, this new penetration is well developed and appears as a dark region due to the accumulation of corrosion products at this location (60 minute photograph).

Subsequent examination of the crevicing in Figure 6 showed that the penetration had an upward thrust as shown schematically in Figure 7, in accord with the i_{\max} current occurring on the upper part of the penetration since this is where the active/passive interface is located. Figure 8 shows a long time consequence of the upward thrust of the penetration. Surface perforations occur, producing the often observed lace-like morphology of surface penetrations around pits and crevices (2,3,21), as the crevice penetrates the surface from underneath. Once the penetration occurs, active dissolution ceases or slows considerably because the large IR drop that supports the active condition vanishes the moment a new, shorter electrolyte path to the bulk solution exists. Thus, these previously active regions now passivate, and the process repeats at the new active/passive interface to produce another penetration and eventually many penetrations as shown in Figure 9. This sequence of events is schematically illustrated in Figure 10. Note that this explanation of these particular dissolution patterns is based on local potential variations rather than on local composition variations. Composition variations, of course, exist but they are a natural consequence of the variation of local electrode potential within the crevice (3); i.e., a new crevice solution composition arises from the corrosion products and the diffusion of ionic species which, themselves further promote, or may even be necessary along with an electrode potential in the active region, for the local cell action to occur, e.g., acidification and/or

Cl^- ion buildup. Results for some metal/electrolyte systems show that both composition changes and potential variations are necessary for localized corrosion to occur, e.g., pitting in iron (6) and crevicing in iron in alkaline solutions (22, 23).

The gas bubbles seen in Figure 6 are hydrogen since this is the only gas that can be generated at the electrode potentials existing in the crevice. Most of the initial bubbles are from the cathodic polarization applied at the beginning; but they grow rather than wane, after the potential is switched to the passive region. Their growth is by molecular diffusion of hydrogen generated in situ. The hydrogen bubbles are seen to grow continuously during anodic polarization, which indicates that the growth is not due to the coalescence of residual hydrogen molecules from the cathodic treatment, but rather is due to the continuous generation of hydrogen molecules deep in the crevice where the potential is appropriate for this reaction.

Typical potential and current transients in the crevice are shown in Figure 11. The electrode potential at the crevice bottom was always at a very low overpotential for metal dissolution, with the value drifting more negative with time after an initial steeper decrease of a few tens of mV. The current was always high, typical of the active region of the polarization curve, and drifted higher with time. To plot the current density shown in Figure 11, the measured current was divided by the total exposed metal area (outer top surface plus crevice wall). Since nearly all the current comes from the much smaller area shown by the bracket in Figure 6, the true crevicing current density is much larger.

Even though the electrode potential in the crevice during active crevicing, has been found from time $t = 0$ to be much more negative than the applied potential at the outer surface, the question remains as to what the electrode potential in the crevice would be if the crevice was inactive, i.e., is there, indeed, a one-to-one correlation between active crevicing and $IR > IR^*$ corresponding to an electrode potential in the cavity that is below the Flade or passivation potential, E_{pass} ?

To answer this question sodium chromate inhibitor was added to the solution. At 0.1M concentration the inhibitor caused the entire crevice wall, rather than just the upper portion, to

passivate (the only exception being areas under attached gas bubbles) and, as needed for the one-to-one correlation, the measured electrode potential everywhere in the crevice, except in the bubble microcrevices where measurements could not be made, was at a much more positive value close to the applied potential. These potential values are shown in Figure 12. For lower concentrations of inhibitor the crevice wall remained active below the active/passive transition just as without inhibitor and the electrode potential in the lower section of the crevice was at a much lower value within the active loop region of the polarization curve. These results prove the existence of a 1:1 correlation between the crevice electrode potential and the occurrence of active crevicing.

This leads to the conclusion that the one requirement that is always necessary for active crevicing, and probably also for pitting of iron based on other data (2,3), is that the electrode potential somewhere in the crevice must be in the active loop region of the polarization curve for the crevice solution. This conclusion is based on the measured electrode potential data given above and the fact that the traditionally reported changes in solution composition associated with localized corrosion were minimized in the present work by using a buffered solution which contained no Cl^- or other aggressive ions. Thus, a potential in the active loop region is not only necessary but also sufficient for crevicing of iron in slightly acidic solutions.

For certain other metal/electrolyte systems this potential condition is found to be necessary but is not in itself sufficient. In these cases, a change in the solution composition within the cavity is also required. Its function, based on a few data (6,22,23), is to shift the E_{flade} or E_{pass} potential to more positive values so that $IR^* > IR$ decreases or even to form an active loop if none otherwise exists, in order that the $IR > IR^*$ condition can be met.

Enhanced Local Cell Action at the Gas Interface and Solution Viscosity

Accumulation of in-place gas on the crevice wall raises additional questions concerning the events occurring in a crevice. A gas bubble is an additional, and not negligible, resistance added to the path of the current flowing between the local cell electrolyte and the bulk solution electrolyte. An effect of the gas is indicated in Figure 3 where the crevicing current is more than

twice as high (as without gas) and the potential variations inside the crevice occur within the region of the gas accumulation although the extent of the interference of the bubble with the potential measurement is unknown. An example of crevicing at the metal-gas-electrolyte interface is shown in Figure 13. The enhanced metal dissolution caused by the bubble produces a trench at the location of the upper boundary of the bubble just below the active/passive interface. A trench appears along the upper limit of the bubble because it is in this zone that the peak currents of the active region occur, i.e., just below the active/passive interface (Fig. 4).

The physical size of the restricted region between the bubble and metal will depend on the characteristics of the metal surface in contact with the bubble, the properties of the electrolyte and the strength of the attraction between the gas bubble and the surface. As a general rule, for aqueous solutions without addition of a surfactant, the minimum separation between the gas bubble and the metal surface is on the order of the thickness of one or two monolayers. This can be considered as a lower boundary for the dimension of the new crevice. Even if the bubble is several monolayers from the solid surface, the crevice dimension is still much smaller than the usual size of pre-existing crevices. The consequence is the creation of a very active local cell in the microcrevice, illustrated in Figure 14, formed by contact of the gas bubble with the metal, where the electrode potential is much less noble than the value existing at the outer surface because of the high IR drop associated with metal dissolution and current flow through the cross section of the micro-crevice of the attached gas bubble.

Figure 15 shows further evidence of the ideas presented in Figure 14. Figure 15a is a photograph of the metal wall in the crevice that is entirely passivated as reported above for the inhibited solution except in the region of the gas bubble. The circle in the center of the photograph corresponds to the location of a hydrogen bubble formed during the cathodic pre-treatment. This entire circular area was actively dissolving but the dark region at the center of the circle underwent the most dissolution, and was probably at the $IR > IR^*$ condition for the longer time. Additional details of the electrochemical conditions in a crevice in the presence of an inhibitor are discussed elsewhere (22,23).

An additional feature appeared in the crevice that relates to the physicochemical characteristics of the electrolyte in it; a remarkable increase in the viscosity was noticed after approximately 20 hours into the experiment. Under this condition oscillation of the attached gas bubbles ceased, as if the bubbles were more tightly bound to the metal. This increase in the viscosity of the solution can be caused by either an increase in the physical interaction (Van der Waals forces, ion-ion, ion-dipole, etc.) between the entities in solution, or to the production of new aggregates originated by chemical interactions (e.g. polynuclear complexes or colloidal particles). In any case, regardless of the origin of the increased viscosity, and given that the mobility of an ion varies inversely with the Stokes viscous force (24), the resistivity of the solution in the crevice increases because the mobility of the ions is reduced.

Role of Gas Bubbles In Nucleation of Localized Corrosion

Another role that a gas bubble can have when the bubble is in-place on the surface is to nucleate local cell action when it otherwise either would not occur or would take longer to occur. Two situations can be considered corresponding to whether or not the surface is initially covered with a passivating layer.

For crevicing of a sample initially free of a passivating layer, the outer surface and the outer portion of the crevice, generally passivate very quickly when anodic protection is applied, whereas elsewhere in the crevice the local electrode potential is in the active loop region of the polarization curve and crevicing starts immediately and continues indefinitely. This is so for deep, narrow crevices with or without the in-place gas bubble shown in Figure 16 a and b, i.e., no discrete nucleation event is needed or occurs in this case.

If, on the other hand, a bubble is attached to a surface that would otherwise passivate under the applied anodic protection, as in Figure 16c, the bubble could maintain the active condition producing pitting or crevicing via the IR drop in the microcrevice satisfying the condition $IR > IR^*$ while the rest of the surface quickly passivates. This situation could almost certainly exist routinely. The most intriguing and least known situation is when gas bubbles adhere to surfaces that are already covered by a stable passive layer. Obviously, the same microcrevice mechanism

could produce film breakdown and pitting or crevicing but the conditions would appear to be less favorable, i.e., the current flowing out of the microcrevice is the very small passive current so that the microcrevice would have to be sufficiently narrow and deep so that the condition, $IR > IR^*$, was still met. Each of the above situations can also be envisioned if the passivating condition is maintained by an oxidant in the bulk electrolyte rather than by anodic polarization.

CONCLUSIONS

The role of IR drops in crevicing was studied on iron under conditions designed to avoid gas constrictions and concentration changes, i.e., gas bubbles were removed at the start of the experiment and the solution contained no Cl^- or other aggressive ions and was buffered. The major conclusions are:

1. A necessary and sufficient condition for crevicing for the metal/solution system used in this study was that the electrode potential somewhere in the crevice is in the active loop of its polarization curve.
2. For the system studied the polarization curve of the crevice solution contained an active/passive transition, rather than merely an active condition, since an active/passive interface was observed on the crevice wall. Its existence also explains the lace-like morphology.
3. An electrode potential in the active region can exist inside a narrow, deep crevice in iron in the absence of aggressive ions or accumulated gaseous and/or solid corrosion products.
4. An accumulation of gas in the cross section of the crevice increases the rate of crevicing and, in principle, can initiate crevicing on otherwise passivated surfaces.
5. The common interface, metal-gas-electrolyte, is often the boundary between active and passive regions of the surface.
6. In view of the present results, the nontraditional potential mechanism of localized corrosion, in which major consideration is given to local potential variations within the cavity, is better supported for metal/electrolyte systems in general.

ACKNOWLEDGMENTS

Financial support by the Office of Naval Research under Contract No. N00014-84K-0201 is gratefully acknowledged. One of us (A.V.) wishes to express his gratitude to the instituto universitario de Tecnologia - Region Capital and to Consejo Nacional de Investigaciones Cientificas y Tecnologicas, both in Venezuela, for the support received.

REFERENCES

1. M. Pourbaix "The electrochemical Basis for Localized Corrosion" in Localized Corrosion, R. W. Staehle, et al. eds. National Association of Corrosion Engineers, Houston, Texas, P. 12, 1974.
2. H. W. Pickering and R. P. Frankenthal, "Mechanism of Pit and Crevice Propagation on Iron and Stainless Steels" in Localized Corrosion, R. W. Staehle, et al., eds., National Association of Corrosion Engineers, Houston, Texas, p. 261, 1974.
3. H. W. Pickering and R. P. Frankenthal, J. Electrochem. Soc., Vol. 119, p. 1297, (1972).
4. H. W. Pickering and A. Valdes, "A Review of the Effect of Gas Bubbles and Cavity Dimensions on the Local Electrode Potentials Within Pits, Crevices and Cracks" in Embrittlement by the Localized Crack Environment, R. P. Gangloff, ed. pp 33-48. Metallurgical Society of AIME, Warrendale, PA, p. 33, 1984.
5. H. W. Pickering, Corrosion, Vol. 42, No. 3, p. 125 (1986).
6. H. W. Pickering, this proceedings, p. ?
7. D. A. Vermilyea and C. S. Tedmon, jr., J. Electrochem. Soc., Vol. 117, p. 437 (1970).
8. T. R. Beck and E. A. Greens II, J. Electrochem. Soc., Vol. 116, p. 177 (1969).
9. B. G. Ateya and H. W. Pickering, J. Electrochem. Soc., Vol. 122, p. 1018 (1975).
10. B. G. Ateya and H. W. Pickering, "Electrochemical Processes Within Cavities and their Relation to Pitting and Cracking" in Hydrogen in Metals, I. M. Bernstein and A. W. Thompson, eds., American Society of Metals, p. 206, 1974.
11. W. D. France, Jr., and N. D. Greene, Jr., Corrosion, Vol. 24, No. 8, p. 247 (1968).
12. H. W. Pickering "The Limiting IR Voltage Within Electrolyte in Cavities during Localized Corrosion and Hydrogen Charging of Metals", in Corrosion and Corrosion Protection, R. P. Frankenthal and F. Mansfeld, eds., The Electrochemical Society, Pennington, N.J., p. 85, 1981.
13. R. E. DeLaRue and C. W. Tobias, J. Electrochem. Soc., Vol. 106, p. 827 (1959).
14. C. W. Tobias, J. Electrochem. Soc., Vol. 106, p. 833 (1959).
15. H. Vogt, Electrochimica Acta, Vol. 26, p. 1311 (1981).
16. J. A. Harrison and A. T. Kuhn, Surface Technology, Vol. 19, p. 249 (1983).
17. Bongenaar-Schlenter, et al., J. Appl. Electrochem., Vol. 15, p. 537 (1986).
18. L. J. J. Janssen and E. Barendrecht, Electrochimica Acta, Vol. 28, p. 341 (1983).
19. H. Vogt, J. Appl. Electrochem., Vol. 14 (1985).
20. P. Sides, in Modern Aspects of Electrochemistry, Vol. 18, R. E. White, J. O'M. Bockris and B. E. Conway, eds., Plenum Press, New York, p. 303, 1986.
21. J. Postlethwaite, B. Huber and D. Makepeace, CORROSION 86, Paper No. 273. National Association of Corrosion Engineers, Houston, Texas, 1986.

22. A. Valdes and H. W. Pickering, to be submitted to the J. Electrochemical Soc.
23. A. Valdes, Ph.D. Thesis, The Pennsylvania State University, 1987.
24. J. O'M. Bockris and A.K.N. Reddy, Modern Electrochemistry, Vol. 1, Plenum Press, New York, p. 471, 1974.

FIGURE CAPTIONS

- Figure 1. Schematic of the sample arrangement; the highlighted surfaces are the iron surfaces in contact with the electrolyte.
- Figure 2. Schematic of the experimental set-up.
- Figure 3. Potential profiles along the iron wall of the crevice, with (shadowed region) and without accumulation of gas at the cross section. Applied potential +0.60 V vs. SCE on the outer (top) surface, 0.5M acetic acid - 0.5 M sodium acetate solution of pH 4.6. Approximate currents flowing out of the crevice were 4.5 and 2.0 mA cm⁻² with and without the gas constriction, respectively.
- Figure 4. Schematic showing that for the outer surface at A, the electrode potential along the cavity changes towards B, in which case the boundaries of the active crevicing cell are the active/passive and limiting potentials (2-6,12).
- Figure 5. Theoretical prediction of the ratio of the conductivity of dispersions of non-conductive spheres of unequal size to the conductivity of the continuous phase as a function of the volume fraction of the spheres (20).
- Figure 6. Views, through the Plexiglas, of the iron wall in the crevice during anodic polarization of the outer (top) iron surface at +0.6 V vs. SCE in 0.5 M acetic acid/0.5 M sodium acetate. Above the line shown by the pointer, the crevice passivates. Iron dissolution is rapid in the region shown by the bracket. Mag. 7X.
- Figure 7. An advance of the active crevicing site, that eventually leads to penetration of the top surface; the shadowed region shows the dissolving crevice surfaces.
- Figure 8. After long times the new crevicing penetration reaches the outer (top) surface, breaking through the surface from underneath.
- Figure 9. (a) Crevicing from underneath causes a network of perforations of the top surface, (b) after some time the undermined section collapses.
- Figure 10. Schematic explanation of the role of IR drop in producing the lace-like morphology of "pits" sometimes observed at crevices and inclusions.
- Figure 11. Potential at the bottom of a gas-free crevice and current as a function of time in the aerated pH five solution. Sample cathodically pre-treated at -1.0 V vs. SCE prior to switch to +0.6 V.
- Figure 12. Electrode potential profiles in the crevice for different concentrations of sodium chromate in the buffered pH 4.6 solution. Cathodic pretreatment at -1.0 V vs SCE. Potential readings after 2.5 hr (0.005M), two hr (0.01M) and three hr (0.1M).
- Figure 13. A gas bubble filling the cross section (a) crevicing occurs along the upper portion of the bubble, (b) applied potential, +0.60 V vs. SCE, on the outer (top) surface, 0.5 M acetic acid - 0.5 M sodium acetate - 5x10⁻³ M sodium chromate solution of pH 4.6. Mag. 7X.
- Figure 14. Initiation of localized corrosion at the site of a gas bubble in the crevice.
- Figure 15. (a) Metal dissolution at the site of a gas bubble adhering to an otherwise passive surface. Sample polarized at -1.0 V vs. SCE in 0.1 M sodium chromate in the pH 4.6 solution, 30X; (b) etched metal where the bubble forms the micro-crevice, 120X.

Figure 16. Schematic illustrating the initiation of localized corrosion by adherent gas bubbles on the surface.

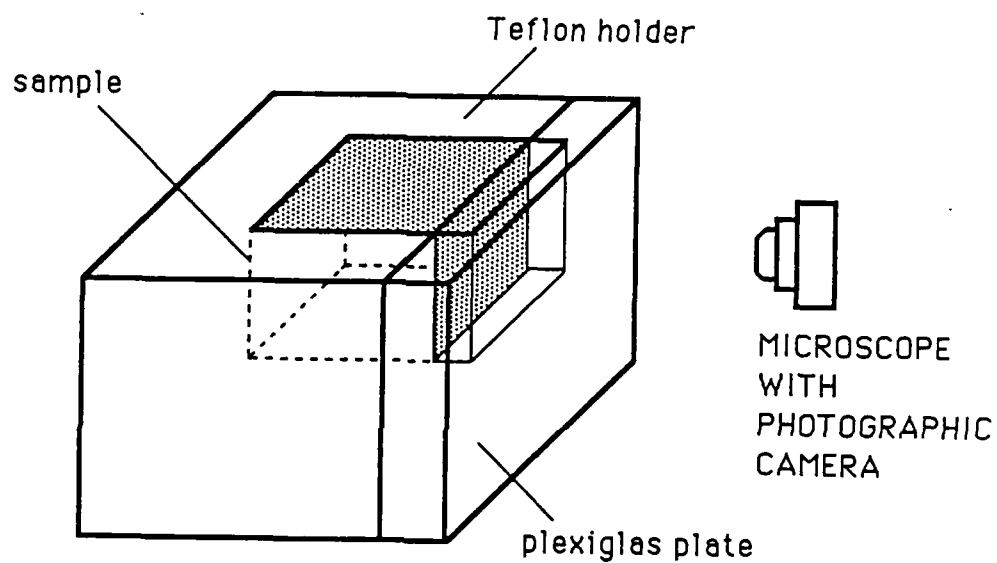


Figure 1. Schematic of the sample arrangement; the highlighted surfaces are the iron surfaces in contact with the electrolyte.

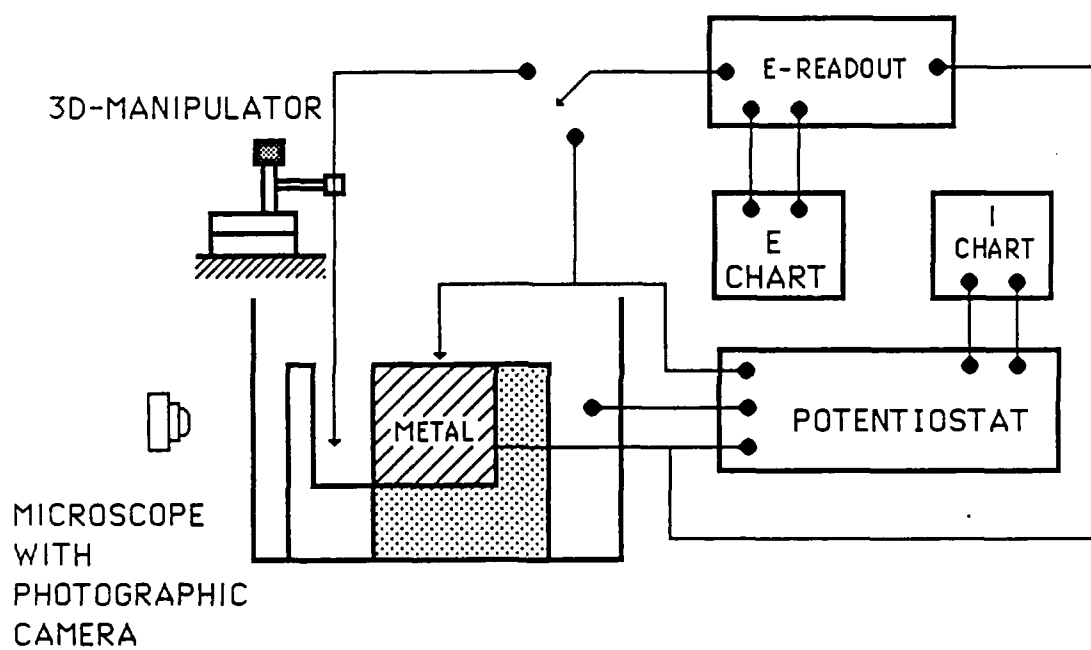


Figure 2. Schematic of the experimental set-up.

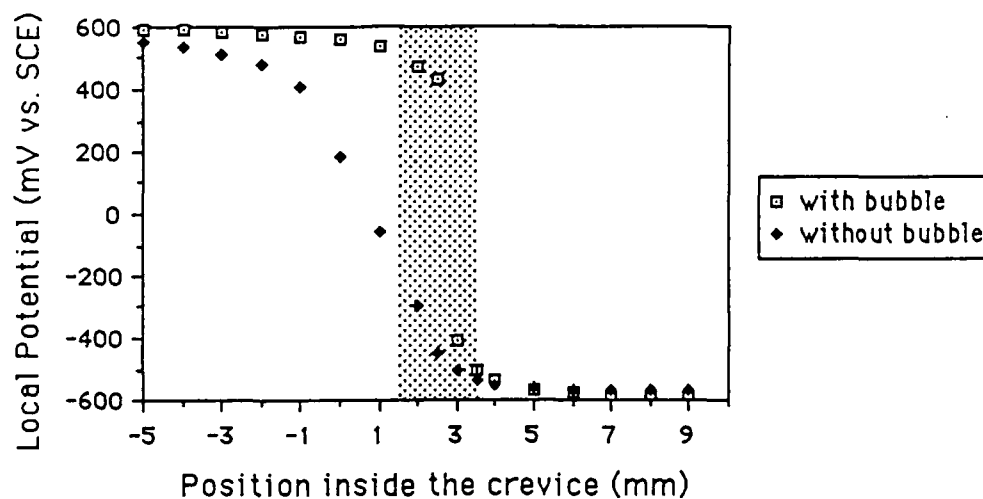


Figure 3. Potential profiles along the iron wall of the crevice, with (shadowed region) and without accumulation of gas at the cross section. Applied potential +0.60 V vs. SCE on the outer (top) surface, 0.5M acetic acid - 0.5 M sodium acetate solution of pH 4.6. Approximate currents flowing out of the crevice were 4.5 and 2.0 mA with and without the gas constriction, respectively.

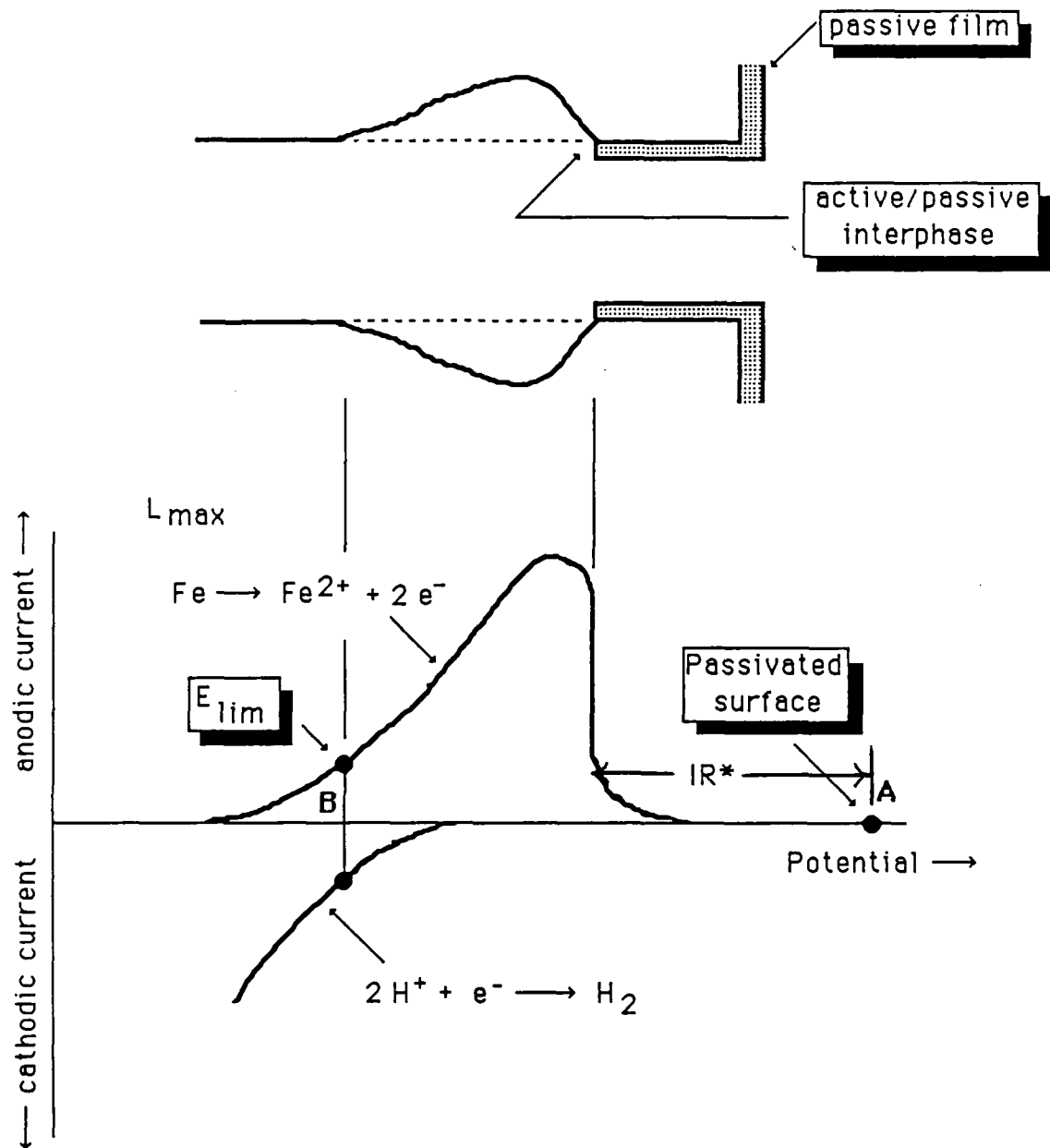


Figure 4. Schematic showing that for the outer surface at A, the electrode potential along the cavity changes towards B, in which case the boundaries of the active crevicing cell are the active/passive and limiting potentials (2-6,12).

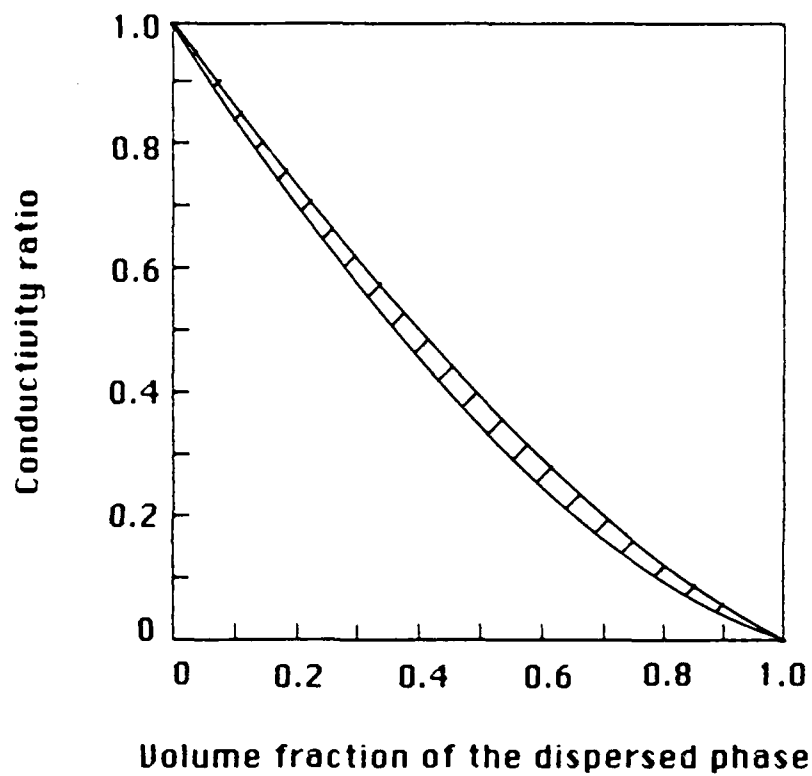
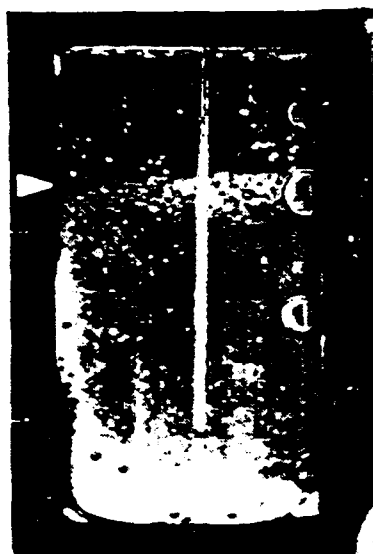
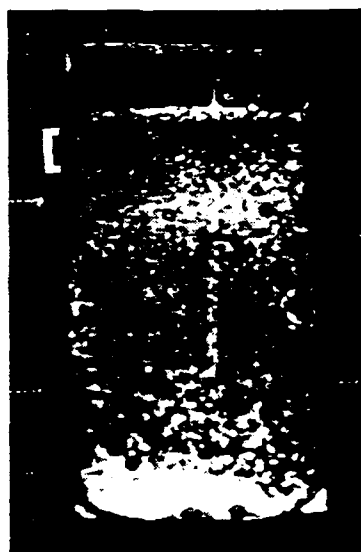


Figure 5. Theoretical prediction of the ratio of the conductivity of dispersions of non-conductive spheres of unequal size to the conductivity of the continuous phase as a function of the volume fraction of the spheres (20).



1 minute



10 minutes



60 minutes

Figure 6. Views, through the Plexiglas, of the iron wall in the crevice during anodic polarization of the outer (top) iron surface at +0.6 V vs. SCE in 0.5 M acetic acid/0.5 M sodium acetate. Above the line shown by the pointer, the crevice passivates. Iron dissolution is rapid in the region shown by the bracket. Mag. 7X.

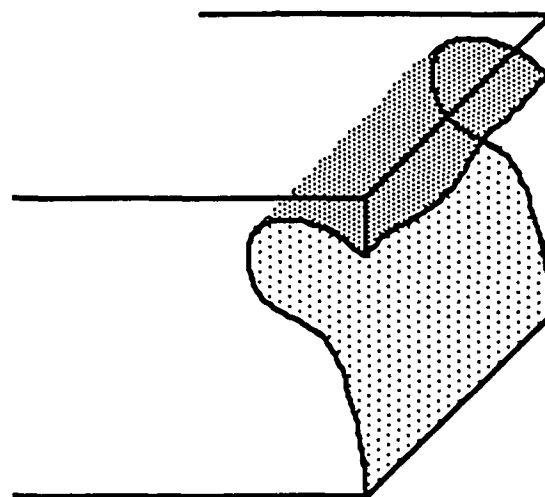


Figure 7. An advance of the active crevicing site, that eventually leads to penetration of the top surface; the shadowed region shows the dissolving crevice surfaces.

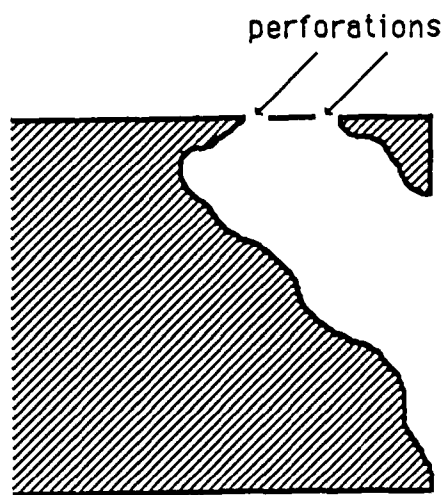
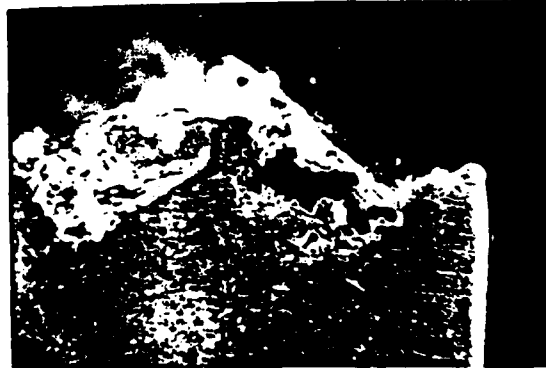


Figure 8. After long times the new crevicing penetration reaches the outer (top) surface, breaking through the surface from underneath.



(a)



(b)

Figure 9. (a) Crevicing from underneath causes a network of perforations of the top surface, (b) after some time the undermined section collapses.

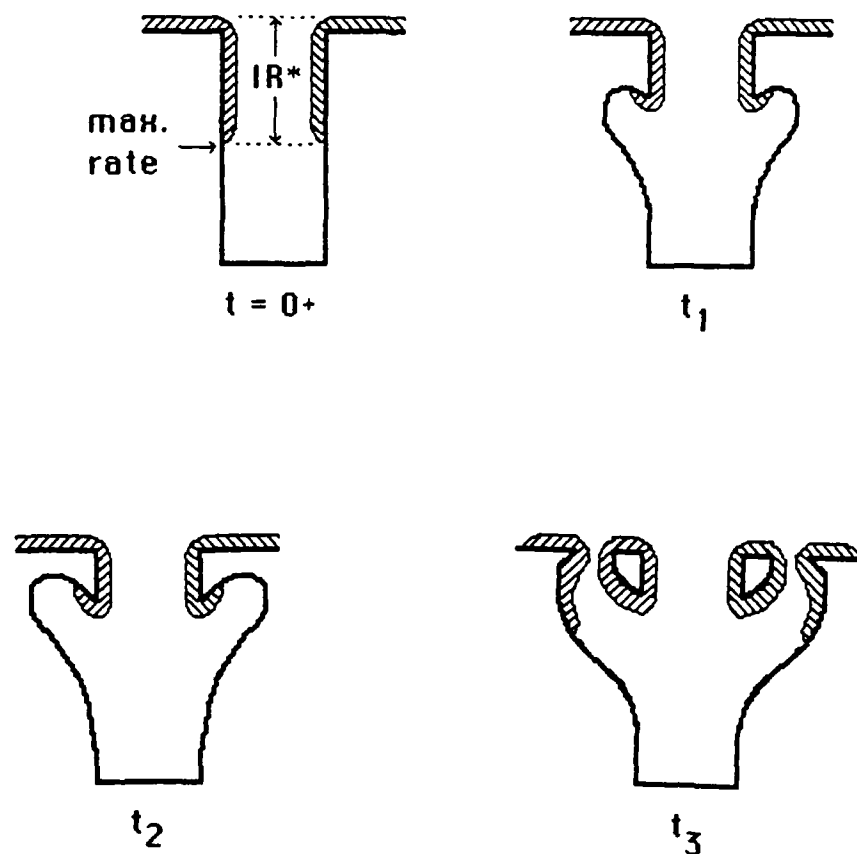


Figure 10. Schematic explanation of the role of IR drop in producing the lace-like morphology of "pits" sometimes observed at crevices and inclusions.

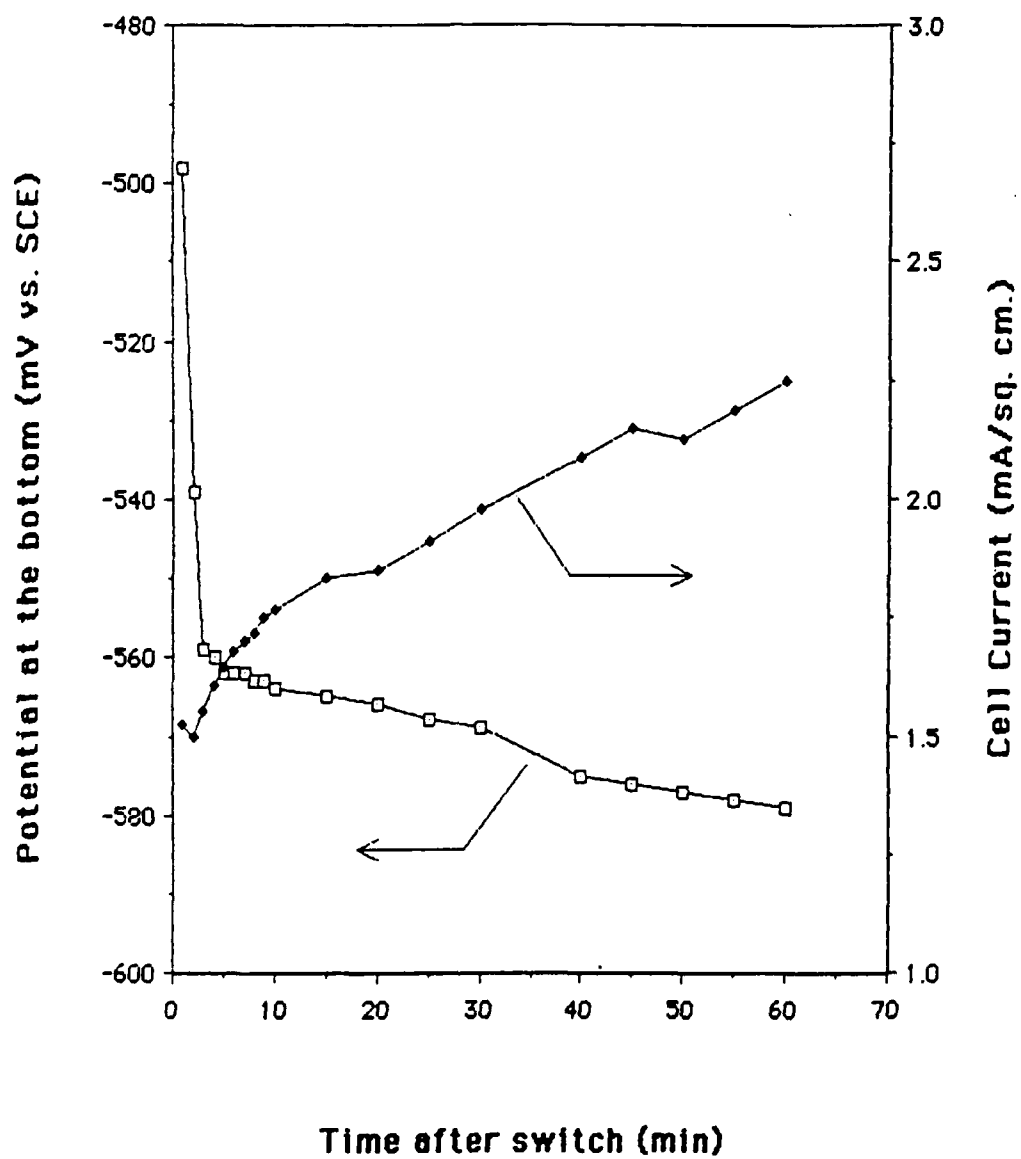


Figure 11. Potential at the bottom of a gas-free crevice and current variation, with time in the aerated pH five solution. Sample cathodically pre-treated at -1.0 V vs. SCE prior to switch to $+0.6$ V.

Local electrode potential (mV vs. SCE)

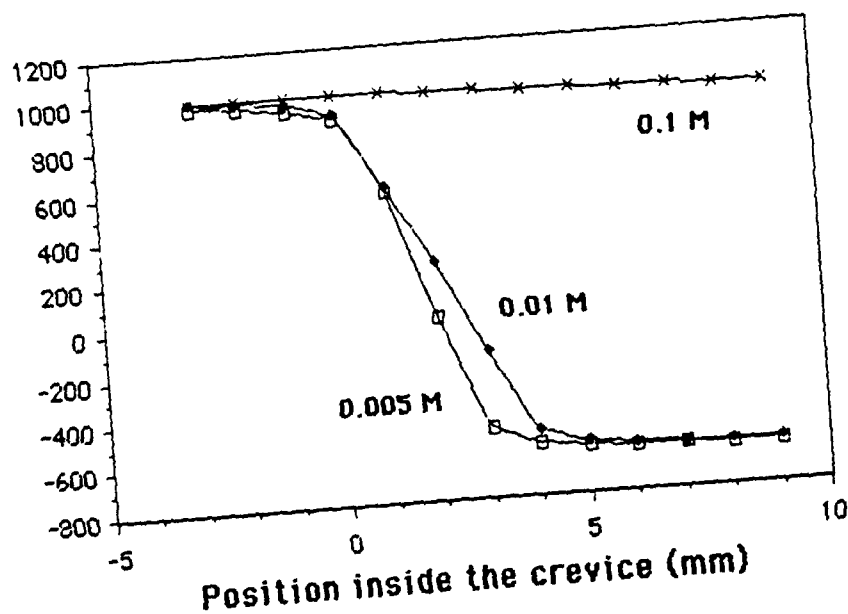


Figure 12. Electrode potential profiles in the crevice for different concentrations of sodium chromate in the buffered pH 4.6 solution. Cathodic pretreatment at -1.0 V vs SCE. Potential readings after 2.5 hr (0.005M), two hr (0.01M) and three hr (0.1M).



Figure 13. A gas bubble filling the cross section (a) crevicing occurs along the upper portion of the bubble, (b) applied potential, +0.60 V vs. SCE, on the outer (top) surface, 0.5 M acetic acid - 0.5 M sodium acetate - 5×10^{-3} M sodium chromate solution of pH 4.6. Mag. 7X.

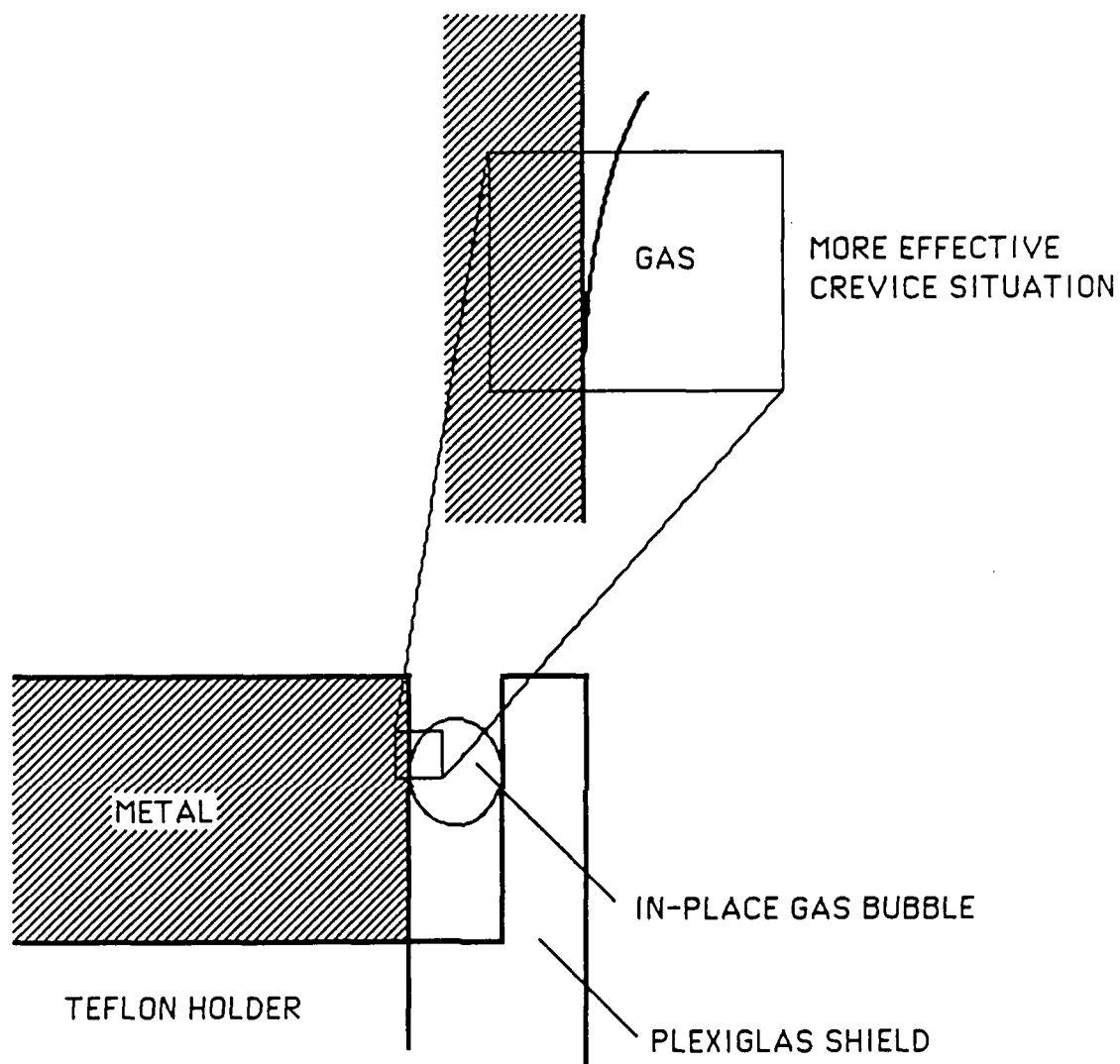
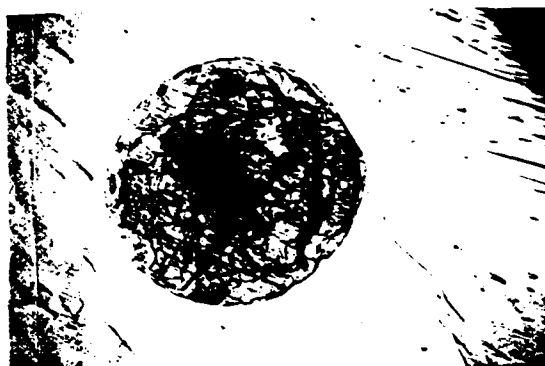


Figure 14. Initiation of localized corrosion at the site of a gas bubble in the crevice.

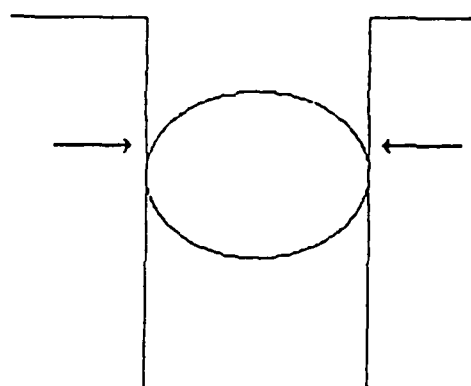


(a)

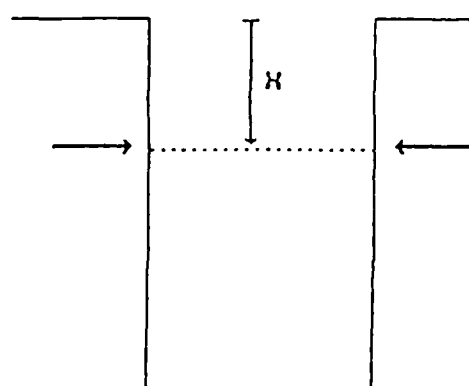


(b)

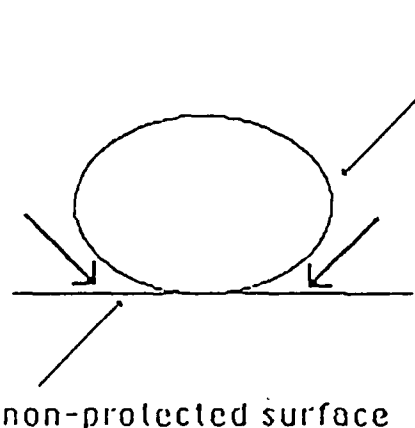
Figure 15. (a) Metal dissolution at the site of a gas bubble adhering to an otherwise passive surface. Sample polarized at -1.0 V vs. SCE in 0.1 M sodium chromate in the pH 4.6 solution, $30\times$; (b) etched metal where the bubble forms the micro-crevice, $120\times$.



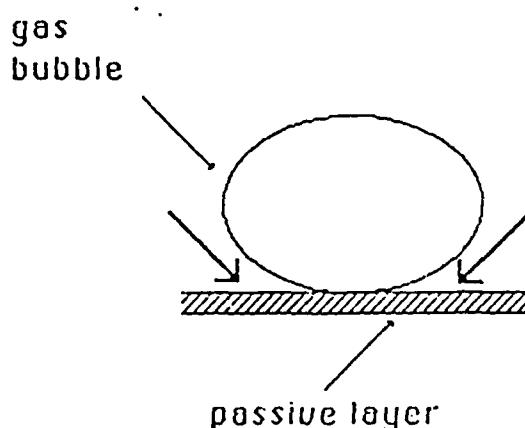
a. enhanced dissolution at the metal-gas-electrolyte interface



b. active condition inside the crevice



c. gas bubble attached to non-protected surface



d. gas bubble attached to protected surface

Figure 16. Schematic illustrating the initiation of localized corrosion by adherent gas bubbles on the surface.

BASIC DISTRIBUTION LIST

Technical and Summary Reports

1985

<u>Organization</u>	<u>Code</u>	<u>Organization</u>	<u>Copies</u>
Defense Documentation Center Cameron Station Alexandria, VA 22314	12	Naval Air Propulsion Test Center Trenton, NJ 08628 ATTN: Library	1
Office of Naval Research Department of the Navy 800 N. Quincy Street Arlington, VA 22217 Attn: Codes 431	3	Naval Electronics Laboratory San Diego, CA 92152 ATTN: Electron Materials Sciences Division	1
Naval Research Laboratory Washington, DC 20375 ATTN: Codes 6000 6300 2627	1 1 1	Naval Missile Center Materials Consultant Code 3312-1 Point Mugu, CA 92041	1
Naval Air Development Center Code 606 Warminster, PA 18974 ATTN: Dr. J. DELuccia	1	Naval Construction Battallion Civil Engineering Laboratory Port Hueneme, CA 93043 ATTN: Materials division	1
Commanding Officer Naval Surface Weapons Center White Oak Laboratory Silver Spring, MD 20910 ATTN: Library	1	Commander David W. Taylor Naval Ship Research and Development Center Bethesda, MD 20084	1
Naval Oceans Systems Center San Diego, CA 92132 ATTN: Library	1	Naval Underwater System Center Newport, RI 02840 ATTN: Library	1
Naval Postgraduate School Monterey, CA 93940 ATTN: Mechanical Engineering Department	1	Naval Weapons Center China Lake, CA 93555 ATTN: Library	1
Naval Air Systems Command Washington, DC 20360 ATTN: Code 310A Code 5304B	1 1	NASA Lewis Research Center 21000 Brookpark Road Cleveland, OH 44135 ATTN: Library	1
Naval Sea System Command Washington, DC 20362 ATTN: Code 05R	1	National Bureau of Standards Washington, DC 20234 ATTN: Metals Science and Stands Division Ceramics Glass and Solid State Science Division Fracture and Deformation Div.	1 1 1

Naval Facilities Engineering
Command
Alexandria, VA 22331
ATTN: Code 03

1

Scientific Advisor
Commandant of the Marine Corps
Washington, DC 20380
ATTN: Code AX

1

Army Research Office
P. O. Box 12211
Triangle Park, NC 27709
ATTN: Metallurgy & Ceramics
Program K

1

Army Materials and Mechanics
Research Center
Watertown, MA 02172
ATTN: Research Programs
Office

1

Air Force Office of Scientific
Research/NE
Building 410
Bolling Air Force Base
Washington, DC 20332
ATTN: Electronics & Materials
Science Directorate

1

NASA Headquarters
Washington, DC 20546
ATTN: Code RRM

1

Mr. Michael T. McCracken
Office of Naval Research Resident
Representative
National Academy of Sciences,
Joseph Henry Bldg.,
Room 623, 2100 Pennsylvania Avenue,
N.W.
Washington, D.C. 20037

1

Defense Metals and Ceramics
Information Center
Battelle Memorial Institute
505 King Avenue
Columbus, Oh 43201

1

Metals and Ceramics Division
Oak Ridge National Laboratory
P.O. Box X
Oak Ridge, TN 37380

1

Los Alamos Scientific Laboratory
P.O. Box 1663
Los Alamos, NM 87544
ATTN: Report Librarian

1

Argonne National Laboratory
Metallurgy Division
P.O. Box 229
Lemont, IL 60439

1

Brookhaven National Laboratory
Technical Information Division
Upton, Long Island
New York 11973
ATTN: REsearch Library

1

Library
Building 50 Room 134
Lawrence Radiation Laboratory
Berkeley, CA

1

Supplemental Distribution List

Jan 1985

Prof. I.M. Bernstein
Dept. of Metallurgy and Materials Science
Carnegie-Mellon University
Pittsburgh, PA 15213

Profs. G.H. Meier and F.S. Pettit
Dept. of Metallurgical and
Materials Eng.
University of Pittsburgh
Pittsburgh, PA 15261

Prof. H.K. Birnbaum
Dept. of Metallurgy & Mining Eng.
University of Illinois
Urbana, Ill 61801

Dr. J.R. Pickens
Martin Marietta Laboratories
1450 South Rolling Rd.
Baltimore, MD 21227-3898

Dr. D.H. Boone
Department of Mechanical Eng.
Naval Postgraduate School
Monterey, Ca 93943

Prof. H.W. Pickering
Dept. of Materials Science and
Eng.
The Pennsylvania State
University
University Park, PA 16802

Dr. C.R. Crowe
Code 6372
Naval Research Laboratory
Washington, D.C. 20375

Prof. R. Summit
Dept. of Metallurgy Mechanics
and Materials Science
Michigan State University
East Lansing, MI 48824

Prof. D.J. Duquette
Dept. of Metallurgical Eng.
Rensselaer Polytechnic Inst.
Troy, NY 12181

Prof. R.P. Wei
Dept. of Mechanical Engineering
and Mechanics
Lehigh University
Bethlehem, PA 18015

Prof. J. P. Hirth
Dept. of Metallurgical Eng
The Ohio State University
Columbus, OH 43210

Prof. A.J. Ardell
Dept. of Materials Science and Eng
School of Engineering & Applied
Science
University of California at
Los Angeles
Los Angeles, CA 90024

Dr. R.G. Kasper
Code 4493
Naval Underwater Systems Center
New London, CT 06320

Prof. B.E. Wilde
Fontana Corrosion Center
Dept. of Metallurgical Eng.
The Ohio State University
116 West 19th Ave.
Columbus, OH 43210

Prof. H. Leidheiser, Jr.
Center for coatings and Surface Research
Sinclair Laboratory, Bld. No. 7
Lehigh University
Bethlehem, PA 18015

Dr. C. R. Clayton
Department of Materials Science
& Engineering
State University of New York
Stony Brook
Long Island, New York 11794

Dr. F. Mansfeld
Rockwell International - Science Center
1049 Camino Dos Rios
P.O. Box 1085
Thousand Oaks, CA 91320

Prof. Boris D. Cahan
Dept. of Chemistry
Case Western Reserve Univ.
Cleveland, Ohio 44106

Dr. K. Sadananda
Code 6390
Naval Research Laboratory
Washington, D.C. 20375

Prof. M.E. Orazem
Dept. of Chemical Engineering
University of Virginia
Charlottesville, VA 22901

Mr. T.W. Crooker
Code 6310
Naval Research Laboratory
Washington, D.C. 20375

Prof. G.R. St. Pierre
Dept. of Metallurgical Eng.
The Ohio State University
Columbus, OH 43210

Prof. G. Simkovich
Dept. of Materials Science & Eng.
The Pennsylvania State University
University Park, PA 16802

Dr. E. McCafferty
Code 6310
Naval Research Laboratory
Washington, D. C. 20375